Dynamic Calibration of Slab Track Models for Railway Applications using Full-Scale Testing

J. Sainz-Aja[1], J. Pombo[2,3], D. Tholken[4], I. Carrascal[1], J. Polanco[1], D. Ferreño[1], J. Casado[1], S. Diego[1], A. Perez[1], J. Abdala Filho[4,5], A. Esen[6], T. Marolt Cebasek[7], O. Laghrouche[6], P. Woodward[8]

[1]*LADICIM (Laboratory of Science and Engineering of Materials), University of Cantabria, Spain*
[2]*Institute of Railway Research, University of Huddersfield, UK*
[3]*IDMEC, Instituto Superior Técnico, Universidade de Lisboa, Portugal and ISEL, IPL, Portugal*
[4]*Mechanical Engineering Graduate Program, Pontifical Catholic University of Paraná, Brazil*
[5]*Civil Engineering Graduate Program, Federal Technological University of Paraná, Brazil,*
[6]*School of Energy, Geoscience, Infrastructure & Society, Heriot-Watt University, UK*
[7]*Faculty of Engineering and Technology, Liverpool John Moores University, UK*
[8]*Institute for High Speed Rail and System Integration, University of Leeds, UK*

ABSTRACT

Research and development of technology for railways has found new impetus as society continues to search for cost effective and sustainable means of transport. This tasks engineers with using the state-of-the-art science and engineering for rolling stock development and advanced technologies for building high performance, reliable and cost-effective rail infrastructures. The main goal of this work is to develop detailed and validated three-dimensional slab track models using a finite element formulation, which include all components of the infrastructure. For this purpose, the parameters of the computational models are identified by performing full-scale tests of the fastening system and of the slab track, including all its material layers. The computational model proposed here is calibrated using this approach and a good agreement is obtained between experimental and numerical results. This work opens good perspectives to use this reliable track model to study the interaction with railway vehicles in realistic operation scenarios in order to assess the dynamic behaviour of the trains and to predict the long-term performance of the infrastructure and of its components.

Keywords: Vehicle-Track Interaction, Track Modelling, Slab Track, Fastening System, Full-Scale Tests.

1. Introduction

The health and long-time performance of the infrastructure is critical in any rail system, not only due to safety aspects but also owing to the high maintenance costs involved. Besides, it is extremely important to minimize any disturbance in the railway service due to the social and economic repercussions. Despite its importance, the performance and maintenance management of the track is, scientifically, one of the least understood and least predictable elements of railway systems. This fundamental understanding is central to reduce the Life-Cycle Costs (LCC) and to increase the safety, capacity and reliability of the rail networks.

During train operation, tracks are subjected to high impact and fatigue loads that can originate rapid degradation and unexpected, unpredictable failure. The conventional approach used by the infrastructure managers consists of performing regular preventive maintenance, fixed lifetime replacement or applying corrective measures when an incident occurs. This approach is neither effective nor economical so health/performance assessment and predictive maintenance has a great

potential for innovation due to the high costs associated. Any efficiency improvement on this would represent a great advantage to the rail industry.

Currently, both ballasted and concrete slab tracks are being used for railways worldwide and it is recognised that both forms have advantages and disadvantages. When compared with ballast tracks, slab systems have advantages from a structural point of view, such as higher lateral and longitudinal stability, no rail buckling and lower sensitivity to differential settlements [1–3]. They have also operational advantages such as lower maintenance needs, lower structure height and not presenting the problems that are associated to ballast shaking and flight [4–7]. On the other hand, slab tracks have some disadvantages associated to the higher installation costs and to the lower noise and vibration absorption provided [4,8]. Due to the overall poor performance of ballast for increased train speeds, the use of concrete slab became more popular and various slab track forms have been produced and tested in recent years [2,5,9].

The analysis of the track structure conditions and its dynamic response has devoted the attention of many researchers aiming to support the rail industry in their developments [10–16]. For this purpose, numerical models have been developed mainly using Multibody (MB) and Finite Element (FE) methodologies. The initial models were 2D based on an elastic foundation formulation [17]. Later, Zhai et al. [18] proposed a 2D numerical model which reproduces the dynamic interaction between a lumped mass vehicle and a discretely supported continuous rail track. This type of model has also been used by other researchers [1,19]. Cai et al [20] proposed a 3D model where the track is considered as a periodic elastically coupled beam system resting on a Winkler foundation and uses spring and dashpot elements to simulate the rail pads and the sleepers. A more recent 3D model was proposed by Poveda et al. [21] to analyse the fatigue life of concrete slabs, which was calibrated with lab tests [22]. Other authors have also proposed co-simulation methodologies between MB and FE formulations in order to study the track structure under realistic trainset loads [23,24]. These developments open the possibility of integrating more detailed wheel-rail contact models [25–31], to consider track irregularities [32,33] and other track singularities [7,13,34–36] in the studies aiming to assess the track performance and degradation evolution [11,37–40] in realistic operation conditions.

Due to the multidisciplinary areas of knowledge involved, all issues involving the complete characterization of the railway infrastructure are complex. Therefore, the use of reliable computational tools that are able to reproduce the dynamic response of the track when subjected to the loads induced by the railway traffic is essential. The numerical models have to represent all the structural layers of the track and the elements that are used to fix and support the rails, namely the fastening system. The main difficulty of building such models is the uncertainty associated to the properties of the layers and components that compose them. In order to overcome this uncertainty, field measurements and laboratory tests can be used to validate the numerical models. Nevertheless, many of the track measurements that are performed by the infrastructure managers are unavailable for scientific use due to industry restrictions/confidentiality. The work proposed here is a contribution in this field by proposing a detailed track model with properties that are calibrated with experimental results obtained in a full-scale test facility.

The material layers have non-linear properties that vary with load conditions, frequency, etc. The fastening system is the component that presents higher non-linearities and this is the reason why dedicated lab experiments on it are performed in this work. It should also be noted that the slab technology has a much more predictable behaviour than the ballast tracks, which have a non-linear performance as they are composed of granular material. In the literature there are authors that use linear elastic material models to describe the constitutive relations of the slab track components [41]. Poveda et al [21] use FE solid elements modelled as linear elastic materials to perform studies on the fatigue life design of concrete slab tracks. Zhu et al [42] show that the bilinear cohesive zone model can be employed to capture the mechanical behaviour of the concrete interface of slab tracks. Ren et al [43] show that when debonding occurs the slab track stops exhibiting linear elastic mechanical response. Zhang et al [44] use viscoelastic parameters in the FE models to better predict the initiation

of interlayer debonding of track structure. El-Ghandour et al [45] use the modal frequencies extracted from the FE model, instead of the nodal degrees of freedom, and uses the floating frame of reference formulation to obtain the elastic response of the track system. Using a non-linear FE formulation in this work would represent a heavy burden to the code and would make it almost impossible to use the validated models for vehicle-track interaction studies.

Several authors have devoted their studies to highlight the importance of the fastenings to the rails' dynamic response. Wei et al. [46] concluded that the properties of the rail pads have a non-linear behaviour and are dependent on the frequency and amplitude of the applied loads. Fenander [47] concluded that the rail pad stiffness increases with the preload and with the frequency, although the effect of the frequency is less relevant. Kaewunruen et al. [48] concluded that the level of preloading have a substantial influence on the natural frequencies and dynamic properties of rubber pads. Wei et al. [49] also showed the influence of the frequency in the pads stiffness especially for the vibrations produced by subways in tunnels. Zhu et al. [50] appreciated an increase in the dynamic stiffness and damping of the rail pads with the increment of the excitation frequency. Carrascal et al. [51] studied the deterioration in the rail pads produced by its normal working conditions and defined a test methodology to determine the dynamic behaviour of railway fastening setting pads in working conditions [52,53].

Other authors have dedicated their research activities to investigate the performance of various parts of the railway track structure and have used experimental tests for the purpose. For example, full-scale model tests with simulated train moving loads hace been developed to explore the dynamic performance and long-term behaviour of concrete slab tracks [4,22,54]. In the case of ballasted track, a two-layer railway track model was developed and tested [55]. Pita et al. [56] and Colaço et al. [57] observed that a low track stiffness value can result in a flexible track with poor load distribution, whereas a high track stiffness can cause greater dynamic overloads on the rail, which induces increased vehicle-track interaction forces that lead to rail defects such as corrugation.

The main goal of this work is to develop and calibrate computational models of slab tracks that can be used for the consistent assessment of the performance and dynamic response of the railway infrastructure when subjected to realistic loads imposed by the rolling stock. The properties of the fastening elements have a noticeable uncertainty as they depend on the material, load, preload produced by the fastening system (toe load), frequency and on the degradation degree of the components. Furthermore, there are also uncertainties associated to the properties of the material layers that compose the slab track structure, such as the subgrade and the different concrete types. The main contribution of this work is that the uncertainties associated to the physical parameters of the material layers and of the components that compose the track system are overcome by performing full-scale tests of the slab track structure and of the fastening system. Such experimental data is used to calibrate the numerical models such that they present a frequency response similar to the real physical models.

It is foreseen that the calibrated slab track model proposed here can be used together with detailed vehicle models, in a co-simulation environment, to study the long-term behaviour of the rail infrastructure. This approach can then be used together with suitable track degradation models to develop decision support tools to promote the implementation of science-based maintenance strategies.

2. Track Experimental Campaign

2.1. GRAFT II: Description of the Test Apparatus

A slab track system is generally composed by a track superstructure and a substructure. The superstructure includes the rail, fastening system, slab track and a concrete supporting layer. The track substructure comprises the roadbed, subgrade and subsoil [4]. The dynamic response of the slab

track depends on the properties of all the different layers [58,59]. In this work full-scale laboratory tests of a slab track system are performed comprising the layers represented in Figure 1, namely subgrade, Frost Protection Layer (FPL), Hydraulically Bonded Layer (HBL), bituminous grout layer, slab track (Max Bögl technology), fastening system (Vossloh 300 system) and the rails.

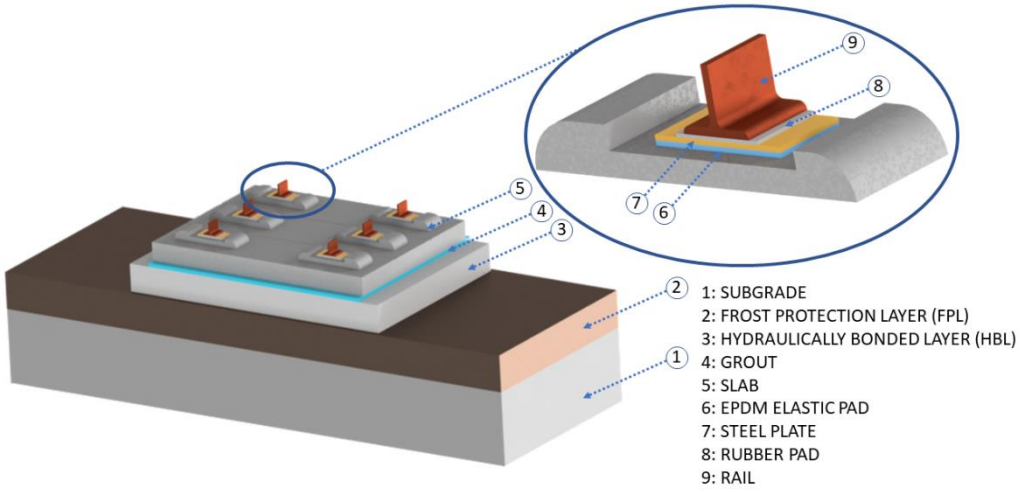

Figure 1 – Representation of the slab track structure

A section of concrete slab track, with all the above mentioned layers, was tested at Heriot-Watt University using the GRAFT II (Geopavement & Railway Accelerated Fatigue Testing) test facility [60], which enables to test full-scale railway tracks under realistic railway loading conditions. This rig operates by using six independent hydraulic actuators that load three full-sized sleepers to simulate the passage of a moving train, by phased loading, with each piston applying loads on a given rail segment. The test apparatus for the slab track test is shown in Figure 2.

Figure 2 – Slab track tests in GRAFT II at Heriot-Watt University

The main characteristics and dimensions of the layers of the slab track tested in GRAFT II are shown in Table 1. The height of the subgrade and FPL is 800 and 400 mm, respectively, corresponding to the German ZTVE-StB 94 standard [61]. In this standard the deflection modulus E_{v2} should be at least 60 and 120 MN/m^2 for the subgrade and FPL, respectively. Laboratory tests found the E_{v2} value of the subgrade to be 67.71 MN/m^2 and 133.55 MN/m^2 for the FPL [60].

Table 1 – Main characteristics and dimensions of the slab track layers

ID	Layer	Description	Dimensions (mm)		
			Width	Length	Height
1	Subgrade	Five layers of compacted sand	6000	2200	800
2	FPL	Sand with higher compacting ratio than subgrade	6000	2200	400

3	HBL	Concrete layer	3000	2100	300
4	Grout	Bituminous grout to increase the elasticity	2550	2100	40
5	Slab and twin block sleepers	Max Bögl slab track system	2550	1930	200
6	EPDM pad	Three layers of the fastening system Vossloh 300	--	--	---
7	Steel plate		--	--	---
8	EVA pad		--	--	---
9	Rail	UIC 60	--	--	---

To analyse the slab track system response, a set of sensors were used, as depicted in Figure 3. These include: (i) One Linear Variable Differential Transformer (LVDT) associated to each one of the six actuators (*ACT 1~6*), to measure the displacement at each loading point; (ii) Four additional LVDTs, to monitor the vertical displacement at the twin block sleepers (*LVDT 1~4*), and; (iii) Three accelerometers to register the accelerations at different points of the slab track system (*ACCEL 1~3*).

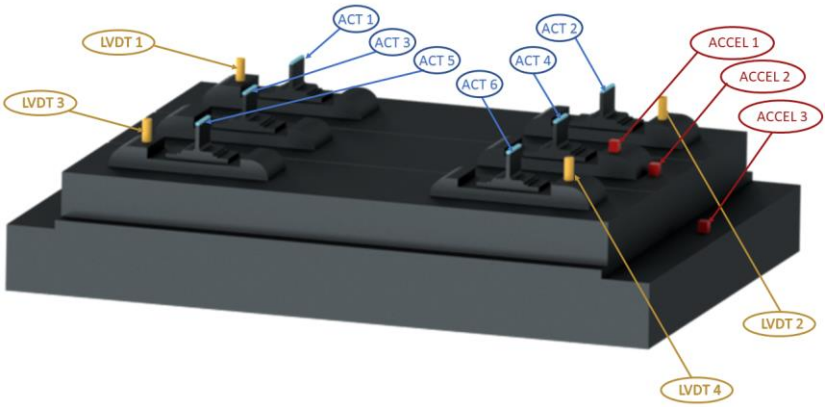

Figure 3 – Location of sensors at the slab track system

The dynamic tests performed on the full-scale slab track were divided in two case studies with load frequencies of 5.6 Hz and 2.5 Hz, corresponding to train speeds of 360 km/h and 160 km/h, respectively. In the high-speed case study (5.6 Hz), three loading scenarios are considered corresponding to different axleloads, as shown in Table 2. In the conventional speed study (2.5 Hz), four axleload scenarios are analysed, as detailed in Table 2.These axleload values are representative of high-speed and conventional trains. Higher frequencies than 5.6 Hz and larger axleloads were not feasible to reach due to the capacity of GRAFT II.

Table 2 – Loading scenarios

Scenario	Axleload (Ton)	Number of Cycles	Frequency (Hz)	Train Speed (km/h)
SC1-1	10.48	1.00×10^3	5.6	360
SC1-2	12.25	1.00×10^3		
SC1-3	13.38	1.17×10^6		
SC2-1	10.64	1.00×10^3	2.5	160
SC2-2	12.68	1.00×10^3		
SC2-3	14.72	1.00×10^3		
SC2-4	16.76	2.20×10^6		

2.2. Experimental Results Post-Processing

The load, displacement and acceleration results, registered by the actuators, LVDTs and by the accelerometers during the laboratory tests, are recorded by the data acquisition system in a discrete manner. In this work, a post-processing procedure is used to obtain an analytical representation of the

sensors data in order to facilitate the comparison of the experimental and numerical results. To this end, a Fourier regression [62,63] is used to find the best fit to an harmonic equation:

$$y(t) = a_0 + a_1.\cos(w.t) + b_1.\sin(w.t) \quad (1)$$

where a_0, a_1 and b_1 are regression parameters and w is the frequency. This equation can be transformed in a typical sinusoidal equation:

$$y(t) = y_0 + A.\sin(w.t + \varphi_0) \quad (2)$$

by using the following relationships [64]:

$$y_0 = a_0 \;\; ; \;\; A = \sqrt{a_1^2 + b_1^2} \;\; ; \;\; \varphi_0 = \arctan\left(\frac{b_1}{a_1}\right) \quad (3)$$

where y_0 is the vertical offset, A is the amplitude and φ_0 is the phase shift of the sinusoidal wave.

Once the Fourier regression is applied to the displacement data recorded by the LVDTs, it is possible to obtain the velocities and accelerations of those points of the track during the experimental tests by the first and second derivatives of equation (2).

As a demonstration of the post-processing procedure used here, a comparison between the loads raw data and the Fourier regression is shown in Figure 4 for scenario SC2-4.

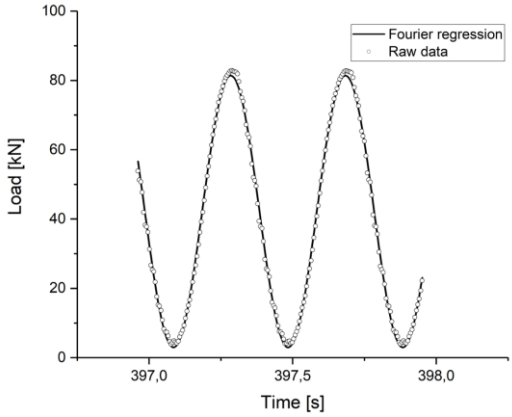

Figure 4 – Example of a Fourier regression

The mean values of the forces registered in the six actuators during the experimental tests are shown in Table 3 for the seven loading scenarios considered here.

Table 3 – Mean values of the forces registered in the actuators

Scenario	F_1 (kN)	F_2 (kN)	F_3 (kN)	F_4 (kN)	F_5 (kN)	F_6 (kN)
SC1-1	42.21	42.22	42.21	42.21	42.20	42.21
SC1-2	42.17	42.20	42.20	42.20	42.20	42.21
SC1-3	42.25	42.25	42.26	42.26	42.23	42.26
SC2-1	42.20	42.21	42.22	42.22	42.21	42.22
SC2-2	42.20	42.20	42.21	42.21	42.21	42.22
SC2-3	42.18	42.20	42.19	42.19	42.19	42.20
SC2-4	42.21	42.20	42.23	42.22	42.23	42.23

The load amplitude of the actuators in the test scenarios is shown in Table 4.

Table 4 – Amplitude of the forces registered in the actuators

Scenario	A_{F1} (kN)	A_{F2} (kN)	A_{F3} (kN)	A_{F4} (kN)	A_{F5} (kN)	A_{F6} (kN)
SC1-1	9.21	9.22	9.22	9.19	9.49	9.38
SC1-2	17.87	17.85	17.83	17.83	18.38	18.23
SC1-3	23.48	23.47	23.41	23.57	24.28	24.16

SC2-1	10.00	10.07	10.01	9.99	10.12	9.99
SC2-2	19.67	19.78	19.74	19.66	19.91	19.81
SC2-3	29.13	29.29	29.24	29.11	29.47	29.36
SC2-4	39.27	39.42	39.49	39.25	39.69	39.66

The vertical displacement and acceleration amplitude registered in the actuators during the experimental tests are shown in Table 5. The values measured in actuators 5 and 6 are discarded as one of the screws failed due to fatigue during the tests and the displacement values were affected by the crack propagation during the fatigue process.

Table 5 – Displacement and acceleration amplitude registered in the actuators

Scenario	ACT 1 (mm)	ACT 2 (mm)	ACT 3 (mm)	ACT 4 (mm)	ACT 1 (mm/s^2)	ACT 2 (mm/s^2)	ACT 3 (mm/s^2)	ACT 4 (mm/s^2)
SC1-1	0.18	0.18	0.18	0.19	218.05	227.38	222.41	233.09
SC1-2	0.38	0.37	0.40	0.37	465.23	462.91	498.68	461.52
SC1-3	0.52	0.50	0.55	0.52	638.37	622.74	677.98	649.26
SC2-1	0.19	0.19	0.23	0.24	46.23	47.71	56.44	59.16
SC2-2	0.45	0.43	0.47	0.48	112.04	105.00	116.29	117.21
SC2-3	0.73	0.68	0.76	0.76	180.61	167.67	187.73	186.64
SC2-4	1.07	1.05	1.10	1.14	264.84	259.37	271.57	280.67

The vertical displacement and acceleration amplitude registered by the four LVDTs during the tests are shown in Table 6.

Table 6 – Displacement and acceleration amplitude registered by the LVDTs

Scenario	LVDT 1 (mm)	LVDT 2 (mm)	LVDT 3 (mm)	LVDT 4 (mm)	LVDT 1 (mm/s^2)	LVDT 2 (mm/s^2)	LVDT 3 (mm/s^2)	LVDT 4 (mm/s^2)
SC1-1	0.007	0.006	0.007	0.008	8.25	7.88	8.94	9.37
SC1-2	0.015	0.014	0.016	0.017	18.54	17.60	19.69	20.89
SC1-3	0.021	0.020	0.022	0.023	25.95	24.50	27.19	28.86
SC2-1	0.008	0.007	0.009	0.010	1.89	1.82	2.16	2.55
SC2-2	0.017	0.017	0.019	0.023	4.26	4.20	4.73	5.61
SC2-3	0.028	0.028	0.030	0.037	6.90	6.84	7.50	9.05
SC2-4	0.040	0.040	0.043	0.052	9.93	9.85	10.57	12.81

3. Fastening System Experimental Campaign

3.1. Description of the Test Apparatus

The rail fastening is the system used to fix the rails to the sleepers that, not only prevents the rails from rotating, but also provide elasticity to the track and damp the transmission of noise and vibrations to the infrastructure resulting from the train operation. The fastening system used in this work is the Vossloh system 300, represented in Figure 5, which is a highly elastic solution for slab track with applications for both conventional and high-speed rail.

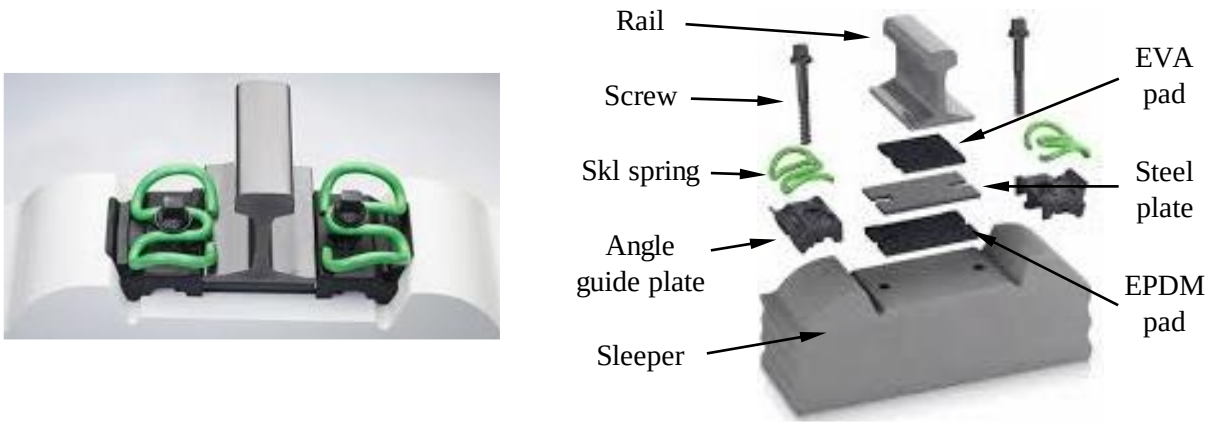

(a) (b)

Figure 5 – Vossloh 300 fastening system: (a) Assembled; (b) Components

As shown in Figure 5(b), the rails are supported by the concrete sleepers through three plates. The top plate, EVA (Ethylene-Vinyl Acetate) shown in Figure 6(a), is a stiff plastic pad that supports the rail foot and insulates it electrically. The intermediate steel plate ensures the distribution of loads from the rail foot and offers tilting protection through its large surface. The bottom plate, EPDM (Ethylene Propylene Diene M-Class) depicted in Figure 6(b), is a synthetic rubber pad that is in contact with the concrete sleeper and offers highly elastic properties to minimize both the vibrations transmitted to the rail supporting structure and the structure-borne noise.

(a) (b)

Figure 6 – Fastening system: (a) EVA pad; (b) EPDM pad

It is well known that the dynamic stiffness of the rail pads depends on the frequency [47,49], on the mean value of the load [48,65] and on the amplitude of the load [46,50]. For this reason, an exhaustive test campaign of the fastening system was performed at the Materials Engineering Laboratory (LADICIM), University of Cantabria, which is accredited to perform this type of studies. The tests, shown in Figure 7(a), were performed according to EN 13146-9:2011+A1:2012 [66] using the same load and the frequency values as the ones used during the full-scale slab track tests.

(a) (b)

Figure 7 – Fastening system tests: (a) General view; (b) LVDTs located in each side of the rail foot

The loads were applied on the rail head during 1000 cycles and the vertical displacements were registered by four LVDTs located in each side of the rail foot, as shown in Figure 7(b). The dynamic stiffness K is calculated according to the expression:

$$K = \frac{\Delta F}{\Delta d} \tag{4}$$

where ΔF and Δd represent the variation of the force and displacement, respectively.

3.2. Laboratory Tests Results

The evolution of the vertical displacement in the loading tests at 5.6 Hz (scenario SC1) and 2.5 Hz (scenario SC2) is shown in Figure 8, where it is evident the influence of the load and of the frequency on the dynamic stiffness of the fastening system.

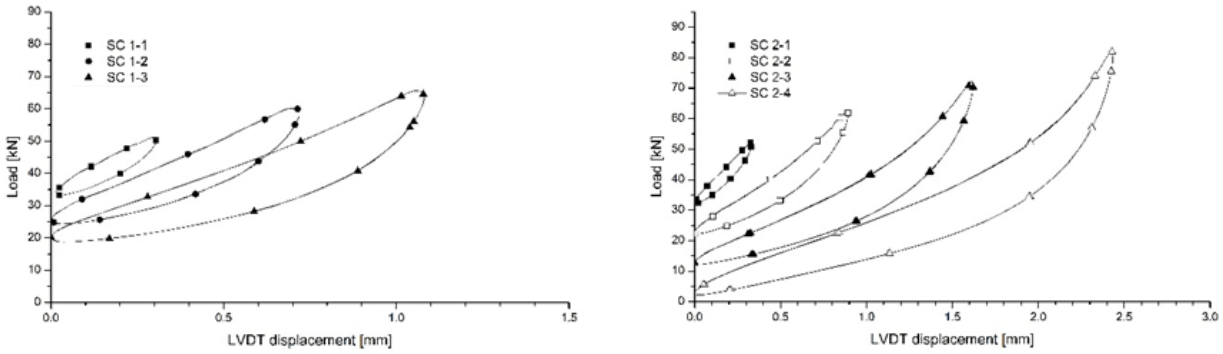

(a) (b)

Figure 8 – Dynamic stiffness tests: (a) Scenario at 5.6 Hz; (b) Scenario at 2.5 Hz

In the full-scale tests that were performed with the slab track, 1.17 million loading cycles were applied in SC1 before starting SC2. Carrascal et al. [53] showed that a 20% increase in the vertical dynamic stiffness of the fastening system occurs in such conditions, especially due to the fatigue deterioration of the EPDM rubber pad. In order to take into consideration this phenomenon, the dynamic stiffness values obtained for the EPDM in the scenarios at 2.5 Hz were increased by 20%, as shown in Table 7 and represented in Figure 9.

Table 7 – EPDM stiffness obtained in the laboratory tests with 20 % correction for 2.5 Hz scenarios

	SC1-1	SC1-2	SC1-3	SC2-1	SC2-2	SC2-3	SC2-4

Frequency [Hz]	5.6	5.6	5.6	2.5	2.5	2.5	2.5
Measured stiffness [kN/mm]	62.97	50.19	43.58	61.1	47.11	36.85	32.06
Corrected stiffness [kN/mm]	62.97	50.19	43.58	73.32	56.53	44.22	38.47

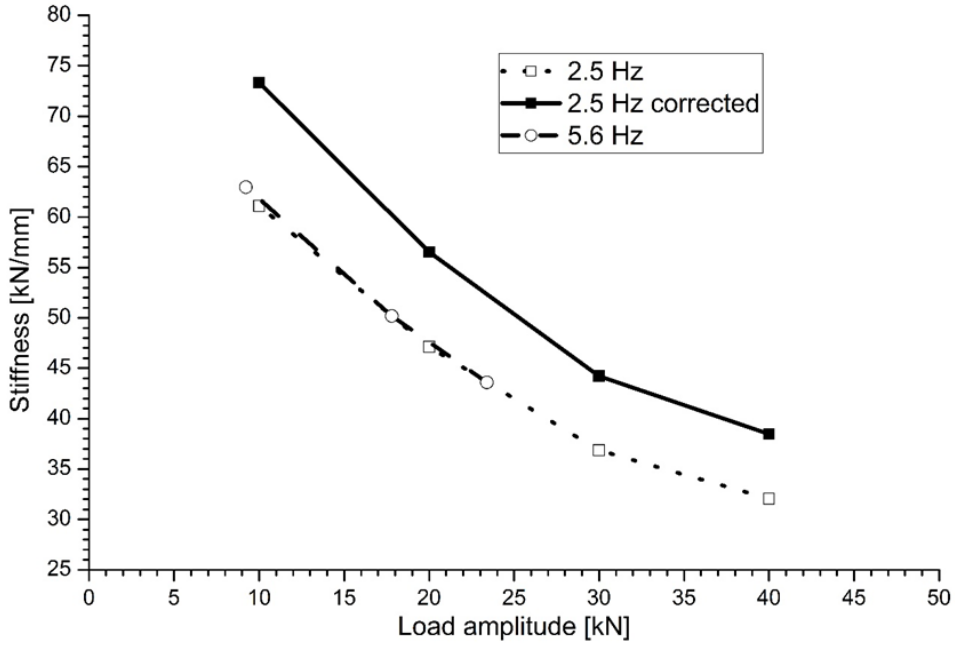

Figure 9 – Dynamic stiffness values obtained in the laboratory tests for the EPDM

4. Slab Track Model

4.1. General Description

The purpose of this work is to develop a detailed and reliable FE slab track model that includes all components of the rail infrastructure. The characteristics of the track layers and of the rail supporting elements are identified by performing full-scale tests of the slab track and of the fastening system as previously described. The FE model is built and studied using the commercial software ANSYS and considering the dimensions shown in Table 1. The dimensions of the fastening system model are depicted in Figure 10.

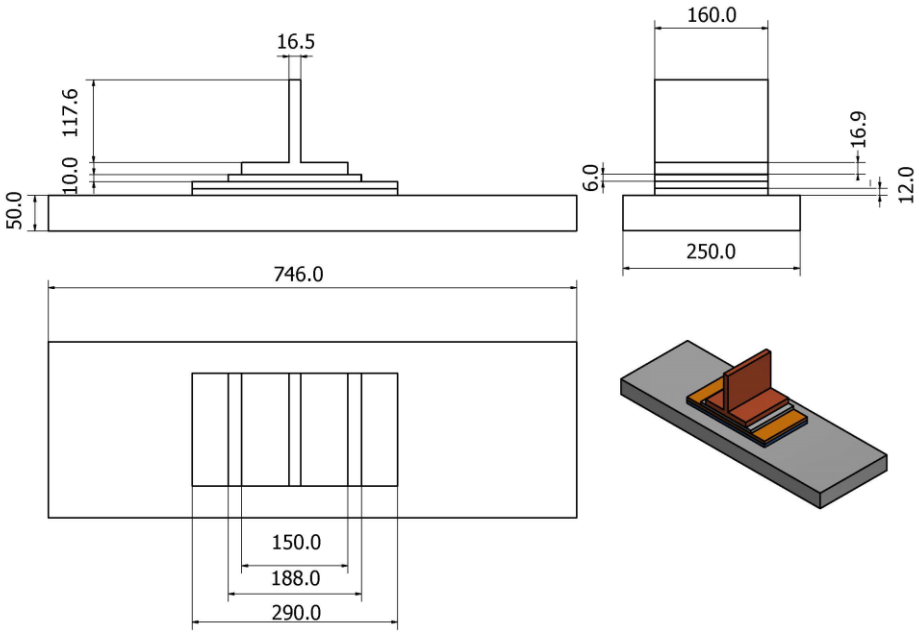

Figure 10 – Fastening system dimensions

Since the study of the stresses distribution on the rails is outside the scope of this work, which is devoted to analyse the dynamic response of the infrastructure, the geometry of the rail cross section is simplified in order to reduce the complexity and size of the FE mesh. The concern here is to guarantee that the dimensions of the rail foot in the model correspond to the dimensions of the rails used in the experiments in order to assure a realistic distribution of loads and stresses to the rail pads.

The boundary conditions of the FE model are considered as fixed support in all lateral faces of the subgrade and of the frost protection layer and at the bottom surface of the subgrade. This is because these layers of material are in contact with GRAFT II metallic plates, as shown in Figure 2.

All contacts between layers are defined as bonded contact, which means that it is considered that there is no sliding or separation between faces or nodes of the model. In order to assure contact compatibility and avoid penetration between elements, an Augmented Lagrange formulation is used as a contact formulation [67].

The calibration of the FE model with the experimental data is performed assuming that all elements are linear and elastic. In this way, the material properties necessary to assemble the model are the density, Young´s modulus and Poisson´s ratio, as shown in Table 8.

Table 8 – Material properties of the slab track model

ID	Layer	Density (kg/m3)	Young's modulus (MPa)	Poisson´s ratio
1	Subgrade	2091	500	0.3
2	Frost protection layer (FPL)	2144	500	0.3
3	Hydraulically bonded layer (HBL)	2400	17870	0.2
4	Grout	2300	22500	0.2
5	Slab and twin block sleepers	2500	36000	0.2
7	Steel plate	7850	Rigid body	
9	Rail	7850	Rigid body	

Due to the variability of the Poisson's ratio in the plastic/rubber materials and the difficulties associated to its calculation, it is proposed here to use the stiffness properties measured during the

fastening system experimental campaign when modelling the EPDM (ID6) and EVA (ID8) pads. The same approach is followed in railway standards [66], which characterize the properties of the fastening systems using stiffness instead of their Young's modulus and Poisson's ratio. The possibility to define the fastening system as an equivalent spring was also analysed here but this idea was discarded as the springs would not distribute uniformely the loads on the FE mesh. Given the above, the EVA and EPDM pads are defined as FE material layers where their properties are defined in such a way that they have the same elastic behaviour as the measured in the experimental tests. Since these pads are much softer than the steel plate, the uniform distribution of loads from the rail foot is assured. The Poisson's ratio of the EVA and EPDM pads is neglected in order to obtain a behaviour similar to a spring. The relationship between the Young´s modulus *E* and the pad stiffness *K* calculated in the fastening system experimental tests is given by:

$$E = \frac{\sigma}{\varepsilon} = \frac{F/A}{\Delta L/L_0} = \frac{F}{\Delta L}.\frac{L_0}{A} = K.\frac{L_0}{A} \tag{5}$$

where *F* is the applied load, *A* is the area of the pad, ΔL is the thickness variation and L_0 is initial thickness of the pad. The properties of the EVA and EPDM pads are shown in Table 9. The stiffness of EVA pads is considered constant and equal to that determined according to the EN standard [66]. The EPDM rail pads are made of a synthetic rubber, which properties vary much more with the amplitude and frequency of the applied loads, requiring the exhaustive laboratory tests performed here to characterize their properties.

Table 9 – Material properties of the EVA and EPDM pads

	SC1-1	SC1-2	SC1-3	SC2-1	SC2-2	SC2-3	SC2-4
EPDM Young's modulus (MPa)	16.29	12.98	11.27	18.96	14.62	11.44	9.95
EPDM density (kg/m3)	1200	1200	1200	1200	1200	1200	1200
EVA Young's modulus (MPa)	397.42	397.42	397.42	397.42	397.42	397.42	397.42
EVA density (kg/m3)	1000	1000	1000	1000	1000	1000	1000

4.2. Mesh Refinement Study

The slab track FE model is built in ANSYS, being the mesh composed by a structured grid with 3D hexahedron elements. The size of these elements is shown in Table 10 for each material layer and depicted in Figure 11.

Table 10 – Mesh dimensions

Layer	Element size (mm)	Refined mesh (mm)
Subgrade	100	50
Frost protection layer	100	50
Hydraulically bonded layer	100	50
Grout	80	40
Slab	40	20
Twin block sleepers	20	10
EPDM PAD	10	5
Steel plate	10	5
EVA PAD	10	5
Rail	15	7.5

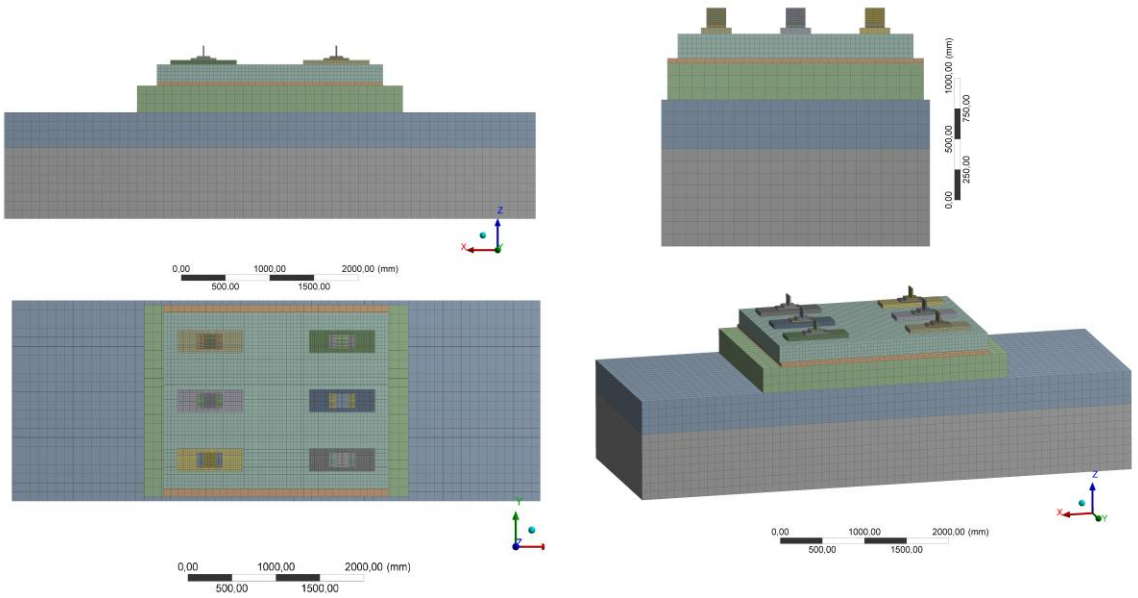

Figure 11 – Finite element mesh

In order to assure a good compromise between computation time and accuracy of the results, a mesh refinement study is performed here by applying 1 kN vertical force to each rail. The purpose is to reduce to half the size of the elements, as shown in Table 10, study the model response and compare the results with the ones from the previous mesh. This process is repeated until a convergence is obtained in the results. Following this approach, the refinement study is performed in six axes of reference, as depicted in Figure 12, representing:

- Axis A: Longitudinal axis in the middle of the model between FPL and HBL.
- Axis B: Transversal axis in the middle of the model between FPL and HBL.
- Axis C: Longitudinal axis in the middle of the model on the top of the slab track.
- Axis D: Transversal axis in the middle of the model on the top of the slab track.
- Axis E: Vertical axis in the central rail.
- Axis F: Vertical axis in the lateral rail.

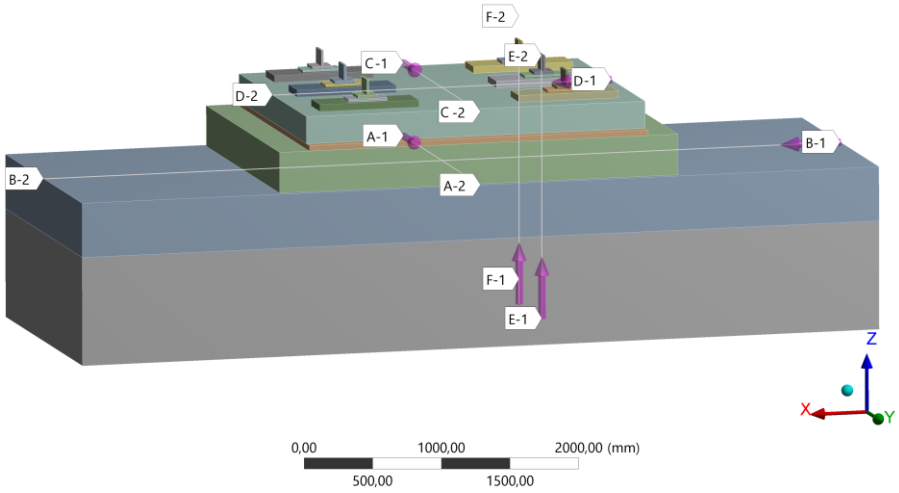

Figure 12 – Axes considered for the mesh refinement study

The comparative study of the vertical displacements on the nodes of the six axes of reference, obtained with the two meshes detailed in Table 10, are shown in Figure 13. The left axes of the plots in this figure represent the displacements, whereas the right axes represent the difference (error) in percentage between the previous and the refined mesh.

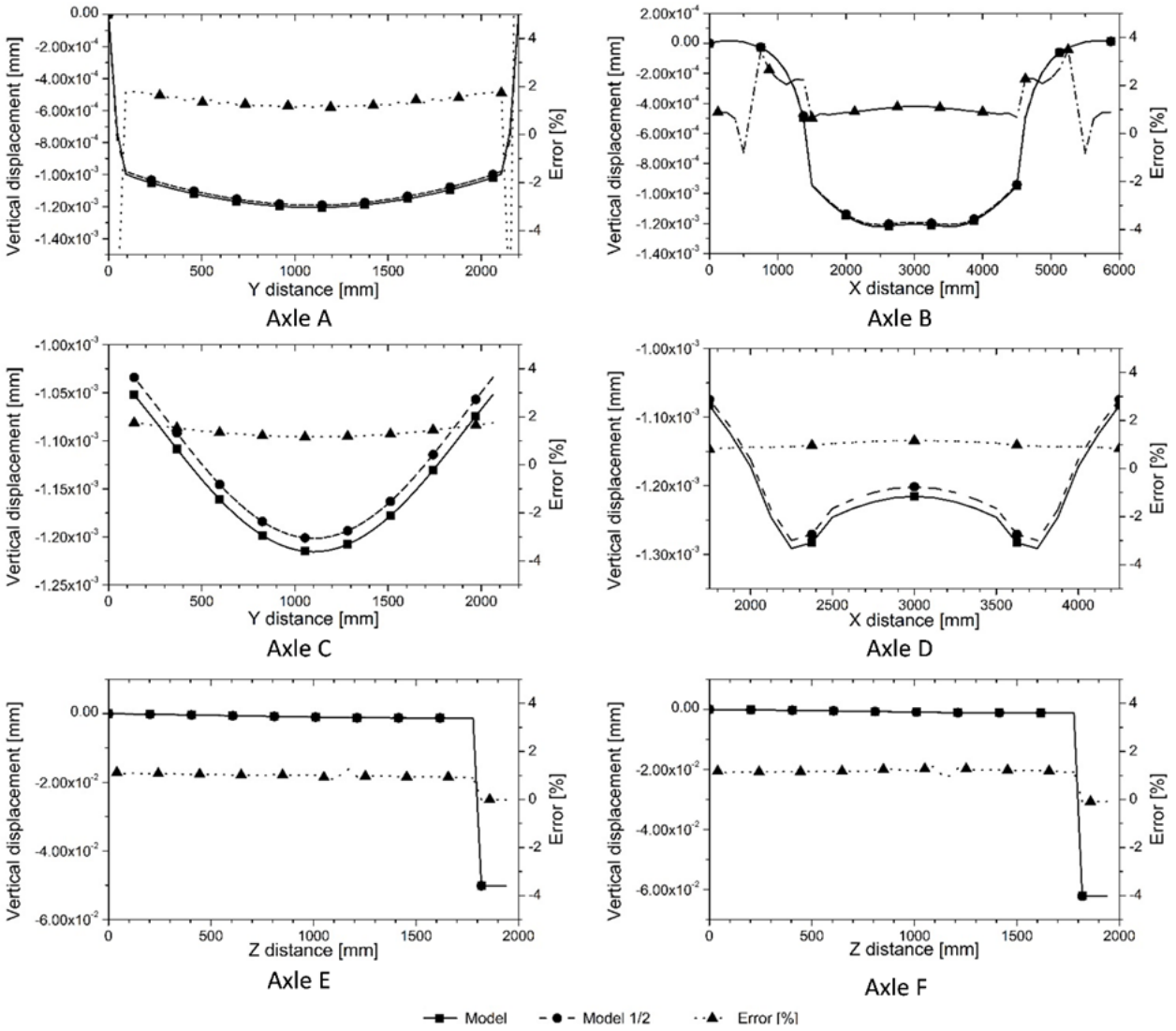

Figure 13 – Refinement study on the six axes of reference: Displacement (left axis); Difference (right axis).

The average difference between nodal displacements along the six axes of reference is shown in Table 11. It is observed that the difference in all axes is lower than 1.5 %. This difference is considered acceptable as the sensors used in the laboratory to measure the vertical displacements are of class 2, which, according to [68], can have a measuring error of up to 2%.

Table 11 – Results of mesh refinement study

Axis	Mean difference (%)
A	1.39
B	1.25
C	0.99
D	1.38
E	0.92
F	1.08

5. Computational Model Calibration

The calibration of the slab track numerical model is performed by comparing the computational results with the ones obtained in the laboratory experiments. To this end, the reference values for the properties of the track material layers are adjusted to get the better possible correspondence between

the numerical and experimental results. The calibrated model considered here is the one with the material properties detailed in Table 8 and Table 9 and the mesh size defined in Table 10.

The comparison of the vertical displacements obtained at the lateral and central rails, named as ACT-1 and ACT-3 respectively in Figure 3, is shown in Figure 14 for the scenario SC1-3 at 5.6 Hz. Homologous results are shown in Figure 15 for the scenario SC2-4 at 2.5 Hz. Only the scenarios representing the higher axleloads are presented here, but the results are similar for the other load conditions studied in this work and detailed in Table 2.

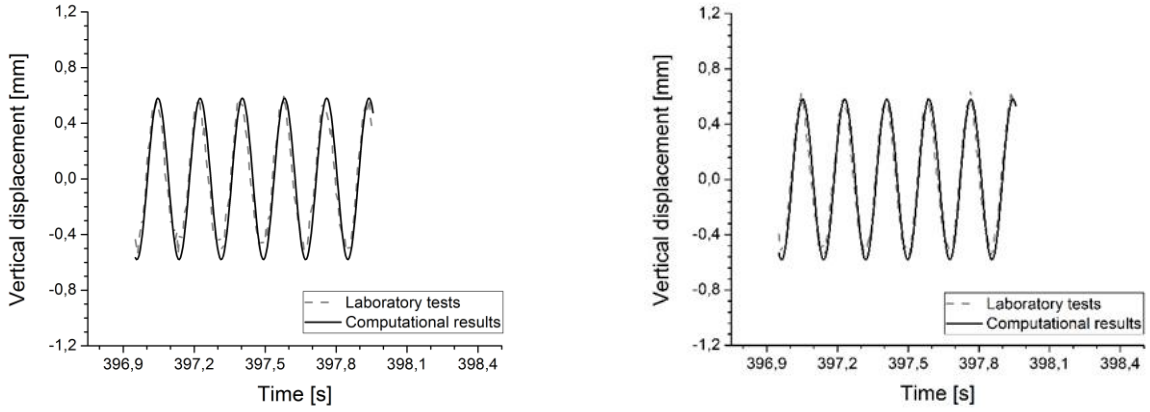

(a) (b)

Figure 14 – Comparison of rails vertical displacement at 5.6 Hz load: (a) Lateral rail; (b) Central rail

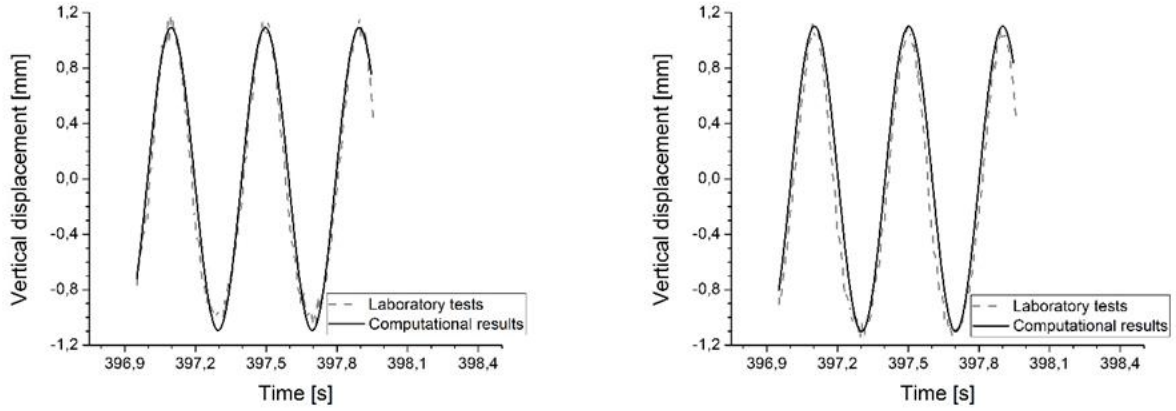

(a) (b)

Figure 15 – Comparison of rails vertical displacement at 2.5 Hz load: (a) Lateral rail; (b) Central rail

Figure 16 presents the comparison of the vertical displacements obtained at the twin block sleepers, named as LVDT-1 and LVDT-3 respectively in Figure 3, for the scenario SC1-3 at 5.6 Hz. Figure 17 presents the homologous results for the scenario SC2-4 at 2.5 Hz.

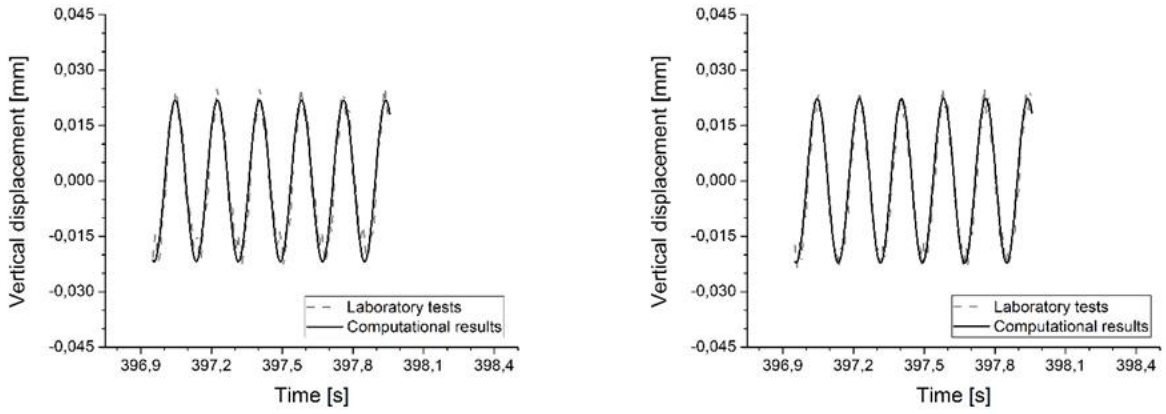

(a) (b)

Figure 16 – Comparison of sleeper vertical displacement at 5.6 Hz load: (a) LVDT-1; (b) LVDT-3

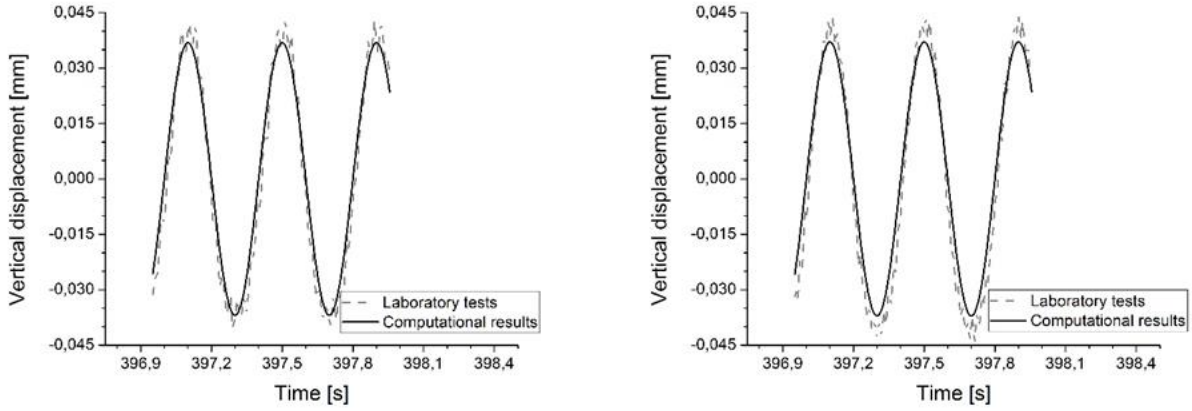

(a) (b)

Figure 17 – Comparison of sleeper vertical displacement at 2.5 Hz load: (a) LVDT-1; (b) LVDT-3

The comparison of the vertical displacement and acceleration amplitudes is shown in Figure 18 and in Figure 19, respectively, for the seven loading scenarios considered in this work. The results are compared at the rails and at the twin block sleepers in such a way that, when there is a point coincident with the 45º line, it represents a full match between the computational results and the experimental tests.

The results presented here reveal a good correlation between the numerical and experimental results in the loading scenarios at 5.6 Hz and at 2.5 Hz. The small differences obtained can be related to several reasons, namely, the materials that compose the slab track structure are not linear and homogeneous as it is admitted in the numerical models. There are also uncertainties associated to the sensors and to the data acquisition system that can contribute for these small variations.

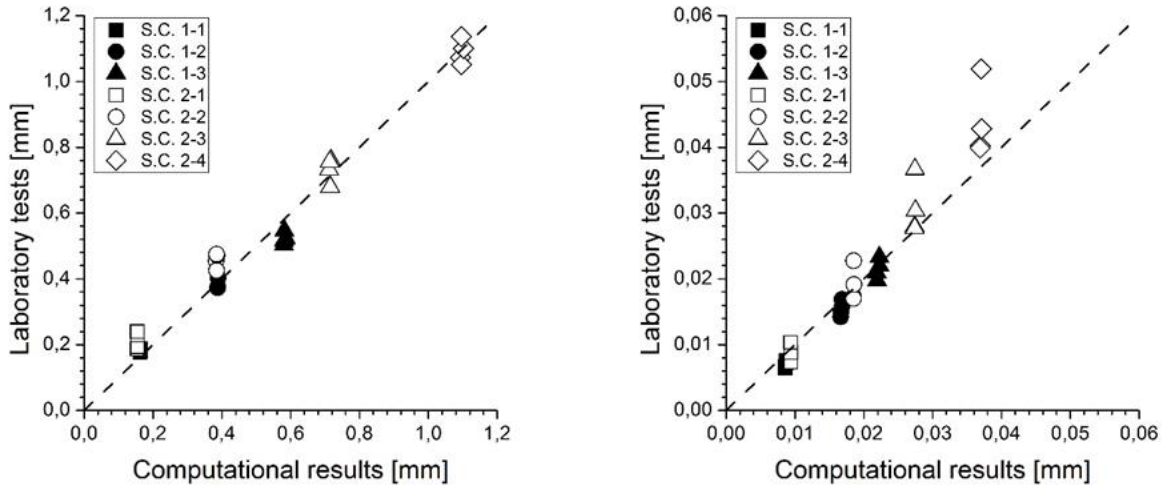

(a) (b)

Figure 18 – Vertical displacement amplitudes: (a) Rails; (b) Twin block sleepers

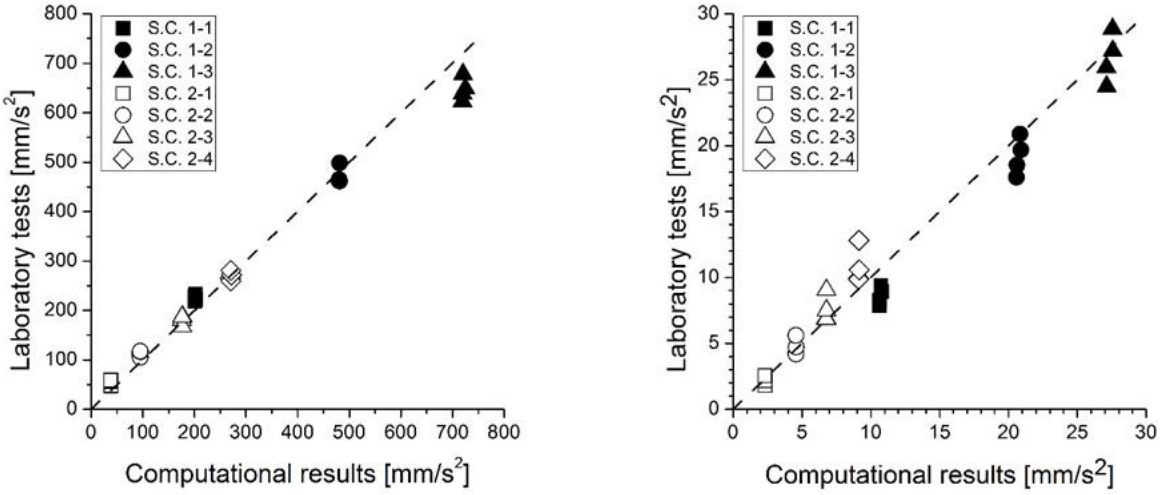

(a) (b)

Figure 19 – Vertical acceleration amplitudes: (a) Rails; (b) Twin block sleepers

6. Conclusions and Future Developments

The aim of this work is to boost the overall performance of rail transport infrastructure by developing reliable numerical models that enable to predict the track behaviour, contributing to reduce the LCC of the infrastructure and to minimize the traffic disruptions, which are mainly caused by unpredicted failures or events. For this purpose, fastening characterization tests and full-scale slab track experiments are performed in realistic operation conditions. Then, a detailed 3D slab track model is built, using the FE program ANSYS, and the properties of all components of the rail infrastructure are calibrated so that the computational model has the same dynamic response as the one obtained in the experimental tests. The results reported here show a good agreement between the numerical and experimental results for the seven load scenarios considered.

Future developments of this work include using the calibrated slab track model to study the long-term behaviour of all elements that compose the infrastructure. Furthermore, this study opens perspectives to study the dynamic behaviour of railway vehicles in realistic scenarios in order to assess the

compatibility between the rolling stock and the track. To this end, it is foreseen the development of a co-simulation procedure between ANSYS, which is used to model the track behaviour, and SIMPACK that is used to analyse the vehicle performance. This advanced vehicle-track interaction methodology can integrate degradation models to promote the development of decision support tools and the implementation of predictive maintenance strategies. This methodology overcomes the limitations of the conventional approach that identifies degradation and deterioration by performing periodic inspections, which are disruptive and not very effective.

Acknowledgements

The authors are grateful to the Engineering and Physical Sciences Research Council (EPSRC) for funding this work under Grant Number EP/NOO9215/1. Tarmac, Tensar and Max-Bögl are also acknowledged for their support with regards to the experimental tests. This work was supported by FCT, through IDMEC, under LAETA, project UID/EMS/50022/2019.

References

[1] Esveld C. Modern Railway Track. MRT-Production, Zaltbommel, The Netherlands; 2001. doi:10.1111/0031-868X.t01-2-00006.

[2] Esveld C. Developments in High-Speed Track Design. IABSE Symp., 2003. doi:10.2749/222137803796328782.

[3] Peltokangas O, Nurmikolu A. Evolution of Railway Track Settlement after Ballast Tamping. Int J Railw Technol 2015;4:1–18. doi:10.4203/ijrt.4.2.1.

[4] Bian X, Jiang H, Cheng C, Chen Y, Chen R, Jiang J. Full-scale model testing on a ballastless high-speed railway under simulated train moving loads. Soil Dyn Earthq Eng 2014;66:368–84. doi:10.1016/j.soildyn.2014.08.003.

[5] Steenbergen MJMM, Metrikine AV, Esveld C. Assessment of design parameters of a slab track railway system from a dynamic viewpoint. J Sound Vib 2007;306:361–71. doi:10.1016/J.JSV.2007.05.034.

[6] Costa D'Aguiar S, Arlaud E, Potvin R, Laurans E, Funfschillling C. Railway Transitional Zones: A Case History from Ballasted to Ballastless Track. Int J Railw Technol 2014;3:37–61. doi:10.4203/ijrt.3.1.2.

[7] Sañudo R, Markine V, Pombo J. Study on Different Solutions to Reduce the Dynamic Impacts in Transition Zones for High-Speed Rail. J Theor Appl Vib Acoust 2017;3:199–222. doi:10.22064/tava.2018.80091.1095.

[8] Woodward PK, Kennedy J, Laghrouche O, Connolly DP, Medero G. Study of railway track stiffness modification by polyurethane reinforcement of the ballast. Transp Geotech 2014;1:214–24. doi:10.1016/j.trgeo.2014.06.005.

[9] Sainz-Aja J, Carrascal IA, Polanco JA, Thomas C, Sosa I, Casado J, et al. Self-compacting recycled aggregate concrete using out-of-service railway superstructure wastes. J Clean Prod 2019;230:945–55. doi:10.1016/j.jclepro.2019.04.386.

[10] Nguyen K, Goicolea JM, Galbadon F. Dynamic effect of high speed railway traffic loads on the ballast track settlement. Congr Métodos Numéricos Em Eng 2011.

[11] Bosso N, Gugliotta A, Zampieri N. A Comprehensive Strategy to Estimate Track Condition and its Evolution. Int J Railw Technol 2012;1:1–19. doi:10.4203/ijrt.1.2.1.

[12] Indraratna B, Nimbalkar S, Rujikiatkamjorn C. Modernisation of Rail Tracks for Higher Speeds and Greater Freight. Int J Railw Technol 2013;2:1–20. doi:10.4203/ijrt.2.3.1.

[13] Fortunato E, Paixão A, Calçada R. Railway Track Transition Zones: Design, Construction, Monitoring and Numerical Modelling. Int J Railw Technol 2013;2:33–58. doi:10.4203/ijrt.2.4.3.

[14] Mezher SB, Connolly DP, Woodward PK, Laghrouche O, Pombo J, Costa PA. Railway critical velocity – Analytical prediction and analysis. Transp Geotech 2016;6:84–96. doi:10.1016/j.trgeo.2015.09.002.

[15] Momoya Y, Nakamura T, Fuchigami S, Takahashi T. Improvement of Degraded Ballasted Track to Reduce Maintenance Work. Int J Railw Technol 2016;5:31–54. doi:10.4203/ijrt.5.3.2.

[16] Woodward PK, Laghrouche O, Mezher SB, Connolly DP. Application of Coupled Train-Track Modelling of Critical Speeds for High-Speed Trains using Three-Dimensional Non-Linear Finite Elements. Int J Railw Technol 2015;4:1–35. doi:10.4203/ijrt.4.3.1.

[17] Pita AL. Estudio de las deformabilidad del sistema balasto-plataforma en una vía férrea bajo la acción de cargas verticales 1976.

[18] Zhai W, Cai Z. Dynamic interaction between a lumped mass vehicle and a discretely supported continuous rail track. Comput Struct 1997;63:987–97.

[19] Knothe KL, Grassie SL. Modelling of Railway Track and Vehicle/Track Interaction at High Frequencies. Veh Syst Dyn 1993;22:209–62. doi:10.1080/00423119308969027.

[20] Cai Z, Raymond GP. Modelling the dynamic response of railway track to wheel/rail impact loading. Struct Eng Mech 1994;2:95–112. doi:10.12989/sem.1994.2.1.095.

[21] Poveda E, Yu RC, Lancha JC, Ruiz G. A numerical study on the fatigue life design of concrete slabs for railway tracks. Eng Struct 2015;100:455–67. doi:10.1016/j.engstruct.2015.06.037.

[22] Tarifa M, Zhang X, Ruiz G, Poveda E. Full-scale fatigue tests of precast reinforced concrete slabs for railway tracks. Eng Struct 2015;100:610–21. doi:10.1016/j.engstruct.2015.06.016.

[23] Antunes P, Magalhães H, Ambrósio J, Pombo J, Costa J. A co-simulation approach to the wheel–rail contact with flexible railway track. Multibody Syst Dyn 2019;45:245–72. doi:10.1007/s11044-018-09646-0.

[24] Pombo J, Almeida T, Magalhães H, Antunes P, Ambrósio J. Finite Element Methodology for Flexible Track Models in Railway Dynamics Applications. Int J Veh Struct Syst 2013;5. doi:10.4273/ijvss.5.2.01.

[25] Muñoz S, Aceituno JF, Urda P, Escalona JL. Multibody model of railway vehicles with weakly coupled vertical and lateral dynamics. Mech Syst Signal Process 2019;115:570–92. doi:10.1016/j.ymssp.2018.06.019.

[26] Pombo J, Ambrósio J, Silva M. A new wheel–rail contact model for railway dynamics. Veh Syst Dyn 2007;45:165–89. doi:10.1080/00423110600996017.

[27] Alonso A, Guiral A, Gimenez JG. Wheel Rail Contact: Theoretical and Experimental Analysis. Int J Railw Technol 2013;2:15–32. doi:10.4203/ijrt.2.4.2.

[28] Pombo J, Ambrósio J. Application of a wheel–rail contact model to railway dynamics in small radius curved tracks. Multibody Syst Dyn 2008;19:91–114. doi:10.1007/s11044-007-9094-y.

[29] Sichani MS, Enblom R, Berg M. Non-Elliptic Wheel-Rail Contact Modelling in Vehicle Dynamics Simulation. Int J Railw Technol 2014;3:77–96. doi:10.4203/ijrt.3.3.5.

[30] Magalhães H, Marques F, Liu B, Antunes P, Pombo J, Flores P, et al. Implementation of a non-Hertzian contact model for railway dynamic application. Multibody Syst Dyn 2019. doi:10.1007/s11044-019-09688-y.

[31] Marques F, Magalhães H, Liu B, Pombo J, Flores P, Ambrósio J, et al. On the generation of

enhanced lookup tables for wheel-rail contact models. Wear 2019;434–435:202993. doi:10.1016/j.wear.2019.202993.

[32] Vollebregt EAH, Steenbergen MJMM. A Methodology for Assessing Track Irregularities with respect to Rail Damage. Int J Railw Technol 2015;4:85–105. doi:10.4203/ijrt.4.4.5.

[33] Pombo J, Ambrósio J. An alternative method to include track irregularities in railway vehicle dynamic analyses. Nonlinear Dyn 2012;68:161–76. doi:10.1007/s11071-011-0212-2.

[34] Hsu SS, Fagan N. Improving Switches and Crossings Performance and Reliability. Int J Railw Technol 2016;5:79–93. doi:10.4203/ijrt.5.3.4.

[35] Coleman I, Kassa E, Smith R. Wheel-Rail Contact Modelling within Switches and Crossings. Int J Railw Technol 2012;1:45–66. doi:10.4203/ijrt.1.2.3.

[36] Hölscher P. The Dynamics of Foundations for High Speed Lines on Soft Soils. Int J Railw Technol 2012;1:147–66. doi:10.4203/ijrt.1.1.7.

[37] Iwnicki SD, Bevan AJ. Damage to Railway Wheels and Rails: A Review of the Causes, Prediction Methods, Reduction and Allocation of Costs. Int J Railw Technol 2012;1:121–46. doi:10.4203/ijrt.1.1.6.

[38] Stichel S, Jönsson P-A, Casanueva C, Hossein Nia S. Modelling and Simulation of Freight Wagon with Special attention to the Prediction of Track Damage. Int J Railw Technol 2014;3:1–36. doi:10.4203/ijrt.3.1.1.

[39] Kuka N, Verardi R, Ariaudo C, Pombo J. Impact of maintenance conditions of vehicle components on the vehicle–track interaction loads. Proc Inst Mech Eng Part C J Mech Eng Sci 2018;232:2626–41. doi:10.1177/0954406217722803.

[40] Pombo J. Application of a Computational Tool to Study the Influence of Worn Wheels on Railway Vehicle Dynamics. J Softw Eng Appl 2012;05:51–61. doi:10.4236/jsea.2012.52009.

[41] Liu S, Chen X, Ma Y, Yang J, Cai D, Yang G. Modelling and in-situ measurement of dynamic behavior of asphalt supporting layer in slab track system. Constr Build Mater 2019;228:116776. doi:10.1016/j.conbuildmat.2019.116776.

[42] Zhu S, Wang M, Zhai W, Cai C, Zhao C, Zeng D, et al. Mechanical property and damage evolution of concrete interface of ballastless track in high-speed railway: Experiment and simulation. Constr Build Mater 2018;187:460–73. doi:10.1016/j.conbuildmat.2018.07.163.

[43] Ren J, Wang J, Li X, Wei K, Li H, Deng S. Influence of cement asphalt mortar debonding on the damage distribution and mechanical responses of CRTS I prefabricated slab. Constr Build Mater 2020;230:116995. doi:10.1016/j.conbuildmat.2019.116995.

[44] Zhang Y, Wu K, Gao L, Yan S, Cai X. Study on the interlayer debonding and its effects on the mechanical properties of CRTS II slab track based on viscoelastic theory. Constr Build Mater 2019;224:387–407. doi:10.1016/j.conbuildmat.2019.07.089.

[45] El-Ghandour A, Foster C. Coupled finite element and multibody systems dynamics modelling for the investigation of the bridge approach problem. Proc Inst Mech Eng Part F J Rail Rapid Transit 2019;233:1097–111. doi:10.1177/0954409719828599.

[46] Wei K, Zhang P, Wang P, Xiao J, Luo Z. The Influence of Amplitude- and Frequency-Dependent Stiffness of Rail Pads on the Random Vibration of a Vehicle-Track Coupled System. Shock Vib 2016;2016:1–10. doi:10.1155/2016/7674124.

[47] Fenander Å. Frequency dependent stiffness and damping of railpads. Proc Inst Mech Eng Part F J Rail Rapid Transit 1997;211:51–62. doi:10.1243/0954409971530897.

[48] Kaewunruen S, Remennikov AM. Laboratory Measurements of Dynamic Properties of Rail Pads under Incremental Preload. 19th Australas. Conf. Mech. Struct. Mater., Christchurch,

New Zealand: Taylor & Francis; 2007, p. 319–24.

[49] Wei K, Wang P, Yang F, Xiao J. Influence of Frequency-Dependent Dynamic Parameters of Rail Pads on Environmental Vibration Induced by Subways in a Tunnel. Transp Res Rec J Transp Res Board 2015;2476:8–14. doi:10.3141/2476-02.

[50] Zhu S, Cai C, Luo Z, Liao Z. A frequency and amplitude dependent model of rail pads for the dynamic analysis of train-track interaction. Sci China Technol Sci 2015;58:191–201. doi:10.1007/s11431-014-5686-y.

[51] Carrascal IA, Casado J, Polanco J, Gutiérrez-Solana F. Dynamic behaviour of railway fastening setting pads. Eng Fail Anal 2007;14:364–73. doi:10.1016/j.engfailanal.2006.02.003.

[52] Ferreño D, Casado J, Carrascal IA, Diego S, Ruiz E, Saiz M, et al. Experimental and finite element fatigue assessment of the spring clip of the SKL-1 railway fastening system. Eng Struct 2019;188:553–63. doi:10.1016/j.engstruct.2019.03.053.

[53] Carrascal IA, Pérez A, Casado J, Diego S, Polanco JA, Ferreño D, et al. Experimental study of metal cushion pads for high speed railways. Constr Build Mater 2018;182:273–83. doi:10.1016/j.conbuildmat.2018.06.134.

[54] Chen R, Zhao X, Wang Z, Jiang H, Bian X. Experimental study on dynamic load magnification factor for ballastless track-subgrade of high-speed railway. J Rock Mech Geotech Eng 2013;5:306–11. doi:10.1016/j.jrmge.2013.04.004.

[55] Anderson WF, Key AJ. Model Testing of Two-Layer Railway Track Ballast. J Geotech Geoenvironmental Eng 2000;126:317–23. doi:10.1061/(ASCE)1090-0241(2000)126:4(317).

[56] Pita AL, Teixeira PF, Robuste F. High speed and track deterioration: The role of vertical stiffness of the track. Proc Inst Mech Eng Part F J Rail Rapid Transit 2004;218:31–40. doi:10.1243/095440904322804411.

[57] Colaço A, Costa PA, Connolly DP. The influence of train properties on railway ground vibrations. Struct Infrastruct Eng 2016;12:517–34. doi:10.1080/15732479.2015.1025291.

[58] Takemiya H, Bian X. Substructure Simulation of Inhomogeneous Track and Layered Ground Dynamic Interaction under Train Passage. J Eng Mech 2005. doi:10.1061/(ASCE)0733-9399(2005)131:7(699).

[59] Kaynia AM, Madshus C, Zackrisson P. Ground Vibration from High-Speed Trains: Prediction and Countermeasure. J Geotech Geoenvironmental Eng 2000;126:531–7. doi:10.1061/(ASCE)1090-0241(2000)126:6(531).

[60] Marolt Čebašek T, Esen AF, Woodward PK, Laghrouche O, Connolly DP. Full scale laboratory testing of ballast and concrete slab tracks under phased cyclic loading. Transp Geotech 2018;17:33–40. doi:10.1016/j.trgeo.2018.08.003.

[61] ZTVE-StB 94. Surface Covering Dynamic Compaction Methods, German Specifications and Regulations, Additional Technical Contractual Conditions and Guidelines for Earthwork in Road Construction and Technical Instructions for Soil and Rock in Road Construction 1994.

[62] Weinstein S, Ebert P. Data Transmission by Frequency-Division Multiplexing Using the Discrete Fourier Transform. IEEE Trans Commun Technol 1971;19:628–34. doi:10.1109/TCOM.1971.1090705.

[63] Mathworks. Fourier Series n.d. https://uk.mathworks.com/help/curvefit/fourier.html (accessed May 17, 2019).

[64] Canuto C, Tabacco A. Serie di Fourier, 2008, p. 77–112. doi:10.1007/978-88-470-0874-8_3.

[65] Kaewunruen S, Remennikov AM. Response and Prediction of Dynamic Characteristics of Worn Rail Pads Under Static Preloads. Proc. 14th Int. Congr. Sound Vib., Cairns, Australia:

Australian Acoustics Society; 2007, p. 1–8.

[66] EN 13146-9:2011+A1:2012. Railway Applications. Track. Test Methods for Fastening Systems. Part 9: Determination of the Stiffness 2012.

[67] Sezer S. An Evaluation of ANSYS Contact Elements. Louisiana State University Master's Theses 60, 2005.

[68] ISO 9513. Metallic materials - Calibration of extensometer systems used in uniaxial testing 2013.